Electronic Supplementary Information

Four isostructural lanthanide metal–organic frameworks: luminescent properties and fluorescence sensing for Fe^{3+} and $Cr_2O_7^{2-}$ ions

Li-Juan Zhao, Bin Li and Guo-Ping Yong*
Department of Chemistry, University of Science and Technology of China, Hefei 230026, P. R. China
E-mail: gpyong@ustc.edu.cn

Table S1 Selected bond distances (Å) and angles (º) for **1**[a].

1	
Eu(1)-O(1)	2.308(3)
Eu(1)-O(3)	2.382(3)
Eu(1)-O(4)#4	2.363(3)
Eu(1)-O(5)#5	2.431(3)
Eu(1)-O(6)#5	2.522(3)
Eu(1)-O(7)	2.426(4)
Eu(1)-O(8)	2.373(3)
Eu(1)-O(9)	2.441(4)
O(1)-Eu(1)-O(3)	85.22(12)
O(1)-Eu(1)-O(4)#4	86.75(11)
O(1)-Eu(1)-O(5)#5	88.36(13)
O(1)-Eu(1)-O(6)#5	75.70(12)
O(1)-Eu(1)-O(7)	75.72(14)
O(1)-Eu(1)-O(8)	144.10(13)
O(1)-Eu(1)-O(9)	147.00(13)
O(3)-Eu(1)-O(4)#4	157.11(12)
O(3)-Eu(1)-O(5)#5	73.02(11)
O(3)-Eu(1)-O(6)#5	121.89(10)
O(3)-Eu(1)-O(7)	78.82(13)
O(3)-Eu(1)-O(8)	70.48(12)
O(3)-Eu(1)-O(9)	120.82(13)
O(4)#4-Eu(1)-O(5)#5	128.14(11)
O(4)#4-Eu(1)-O(6)#5	76.43(10)
O(4)#4-Eu(1)-O(7)	78.43(13)
O(4)#4-Eu(1)-O(8)	105.37(13)
O(4)#4-Eu(1)-O(9)	75.53(13)
O(5)#5-Eu(1)-O(6)#5	52.44(10)
O(5)#5-Eu(1)-O(7)	148.67(15)
O(5)#5-Eu(1)-O(8)	108.26(14)
O(5)#5-Eu(1)-O(9)	81.46(14)
O(6)#5-Eu(1)-O(7)	142.65(12)
O(6)#5-Eu(1)-O(8)	139.60(13)
O(6)#5-Eu(1)-O(9)	73.21(12)
O(7)-Eu(1)-O(8)	73.96(15)
O(7)-Eu(1)-O(9)	125.78(15)
O(8)-Eu(1)-O(9)	68.53(13)

[a] Symmetry code: #4= -x+1, y+1/2, -z+1/2, #5 = -x, -y, -z.

Table S2 The comparison this work with recently published articles related to sensing

analytes	**Ln-MOFs**	solvents	quenching constants **Ksv (M^{-1})**	detection limits （**μM**）	references
Fe^{3+}	**1**	H_2O	8.31×10^3	6.93	*This Work*
	2	H_2O	5.63×10^3	26.11	*This Work*
	3	H_2O	2.86×10^4	1.72	*This Work*
	4	H_2O	1.50×10^4	3.63	*This Work*
	[Eu(BCB)(DMF)]·$(DMF)_{1.5}(H_2O)_2$	H_2O	2.35 ×10^4	1.78	[1]
	$[Eu(PMBB)_{1.5}(H_2O)_2]$	H_2O	3.66×10^3	2.09	[2]
	$[Tb(PMBB)_{1.5}(H_2O)_2]$	H_2O	3.53×10^3	2.22	
	$[Tb_4(TATB)_2]$	H_2O	5.95×10^3	4.84	[3]
	$\{[Eu(qptca)_{1/2}(H_2qptca)_{1/2}(H_2O)_2]\cdot DMF\}n$	H_2O	2.28×10^3	6.45	[4]
	$[Eu_3(BDC)_{4.5}(H_2O)(DMF)_2]$	H_2O	1.30×10^5	11.53	[5]
	$[Tb(tftba)_{1.5}(phen)(H_2O)]n$	H_2O	4.04×10^4	12.70	[6]
	$\{[Eu(dpc)(2H_2O)]\cdot(Hbibp)_{0.5}\}n$	DMF	4.84×10^3	13.20	[7]
	$[Eu_4(pta)_5(Hpta)_2(H_2O)_4]\cdot 9H_2O$	H_2O	1.12×10^4	35.00	[8]
	$[Tb(Hpta)(C_2O_4)]\cdot 3H_2O$	H_2O	1.22×10^4	26.00	
$Cr_2O_7^{2-}$	**1**	H_2O	1.04×10^4	5.11	*This Work*
	2	H_2O	1.37×10^4	1.97	*This Work*
	3	H_2O	2.31×10^4	1.71	*This Work*
	4	H_2O	2.85×10^4	2.10	*This Work*
	$[Eu(PMBB)_{1.5}(H_2O)_2]$	H_2O	7.18×10^3	1.07	[2]
	$[Tb(PMBB)_{1.5}(H_2O)_2]$	H_2O	1.06×10^4	0.74	
	[Zn(4-dptb)(2,2′-bha)]·$4H_2O$	H_2O	2.84×10^3	1.43	[9]
	[Cd(4dptb)(4,4′odpa)$(H_2O)_2$]·H_2O	H_2O	1.85×10^3	4.46	
	Eu-MOF(H_3L)	H_2O	1.29×10^4	1.95	[10]
	[Cd(DPTTZ) (5-AIP)]	H_2O	3.31×10^4	2.60	[11]
	Tb-MOF(H_2atdbc)	H_2O	8.5×10^3	2.92	[12]
	$\{[Cd_2(TFBA)(bibp)_2H_2O]\cdot DMF\cdot 2H_2O\}n$	H_2O	6.73×10^5	3.60	[13]
	$\{[Eu(dpc)(2H_2O)]\cdot(Hbibp)_{0.5}\}n$	DMF	3.97×10^3	10.10	[7]

[Tb(tftba)$_{1.5}$(phen)(H_2O)]n	H_2O	2.86×10^4	18.00	[6]

H_3BCB = 4,4',4''-benzenetricarbonyltri-benzoic acid;
H_2PMBB = 4,4'-((1,4- phenylenebis(methylene))bis(oxy))dibenzoic acid;
H_3TATB = 4,4',4"-(1,3,5-triazine-2,4,6-triyl)tribenzoic acid;
H_4qptca = [1,1':4',1'':4'',1''':4''',1''''-quinquephenyl]-2,2'',2'''',5''-tetracarboxylic acid;
H_2BDC = 1,4-benzenedicarboxylic acid;
phen = 1,10-phenanthroline; H_2tftba = 2,3,5,6-tetrafluoroterephthalic acid;
H_4dpc = 2-(3',4'-dicarboxylphenoxy)isophthalic acid; bibp = 4,4'-bis(imidazolyl) biphenyl;
H_2pta = 2-(4-pyridyl)terephthalic acid; $H_2C_2O_4$ = oxalic acid;
4-dptb = N^3,N^4-bis(pyridine-4-ylmethyl)thiophene-3,4-dicarboxamide; 2,2′-H2bha = 2,2′-biphenyl acid; 4,4′-H2odpa = 4,4′-oxybisbenzoic acid;
H_3L = 4,4′,4″-triazine-2,4,6-tribenzoic acid;
5-AIP = 5-Aminoisophthalic acid; DPTTZ = 2, 5-di(pyridine-4-yl) thiazolo[5,4-d]thiazole;
H_2atdbc = 4,4'-(4-amino-1,2,4-triazol-3,5-diyl)dibenzoic acid;
H_3TFBA = tris(3'-F-4'-carboxybiphenyl)amine; bibp = 4,4'-Di(1H-imidazole-1-yl)-1,1'-biphenyl.

References

[1] M. Y. Zhang, F. Y. Yi, L. J. Liu, G. P. Yan, H. Liu and J. F. Guo, *Dalton Trans.*, 2021, **50**, 15593-15601.

[2] Z. D. Zhou, C. Y. Wang, G. S. Zhu, B. Du, B. Y. Yu, C. C. Wang, *J. Mol. Struct.*, 2022, **1251**, 132009.

[3] X. F. Zhang, L. H. Feng, S. Y. Ma, T. F. Xia, F. F. Jiao, Z. Kong, X. Duan, *J. Solid State Chem.*, 2022, **312**, 123232.

[4] J. Q. Wu, X. Y. Ma, C. L. Liang, J. M. Lu, Q. Shi and L. X. Shao, *Dalton Trans.*, 2022, **51**, 28902-897.

[5] J. J. Zhao, P. Y. Liu, Z. P. Dong, Z. L. Liu, Y. Q. Wang, *Inorg. Chim. Acta.*, 2020, **511**, 119843.

[6] H. H. Yu, J. Q. Chi, Z. M. Su, X. Li, J. Sun, C. Zhou, X. L. Hu and Q. Liu, *CrystEngComm*, 2020, **22**, 3638-3643.

[7] Y. Du, H. Y. Yang, R. J. Liu, C. Y. Shao and L. R. Yang, *Dalton Trans.*, 2020, **49**, 13003-13016.

[8] L. J. Duan, C. C. Zhang, P. P. Cen, X. Y. Jin, C. Liang, J. H. Yang and X. Y. Liu, *CrystEngComm*, 2020, **22**, 1695-1704

[9] X. L. Wang, Y. Wang, N. Xu, J. X. Ma and G. C. Liu, *CrystEngComm*, 2023, **25**, 1186-1192.

[10] Y. X. Sun, G. Guo, W. M. Ding, W. Y. Han, J. Li and Z. P. Deng, *CrystEngComm*, 2022, **24**, 1358-1367.

[11] A. K. Hosseini, Y. Pourshirzad, A. Tadjarodi, *J. Solid State Chem.*, 2023, **317**, 123676.

[12] J. X. Li, B. Q. Yu, L. H. Fan, L. Wang, Y. C. Zhao, C. Y. Sun, W. J. Li, Z. D.

Chang, *J. Solid State Chem.*, 2022, **306**, 122782.
[13] J. Ru, R. F. Zhang, Y. X. Wang, X. X. Ma, Q. Gu, X. M. Du, L. L. Li, Y. L. Wang, *J. Solid State Chem.*, 2022, **311**, 123119.

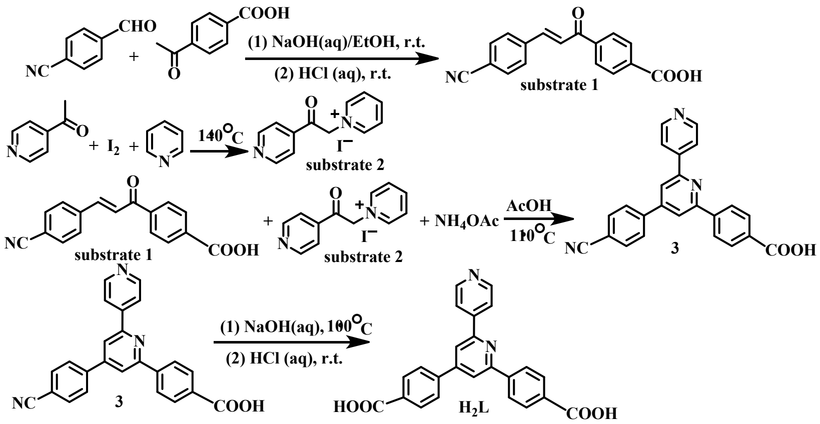

Scheme S1 The synthesis procedure for H_2L ligand.

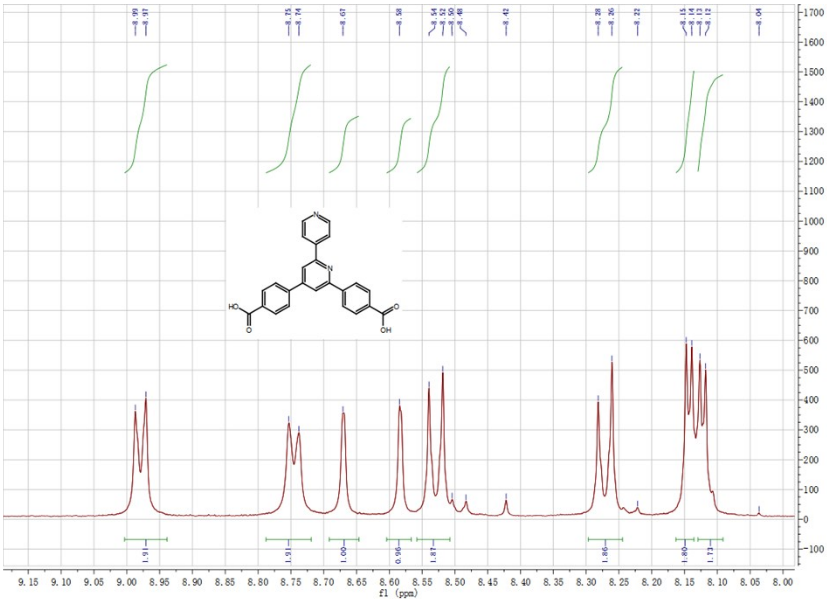

Fig. S1 ^{1}H NMR (400 MHz, dmso-d_6) of H_2L ligand.

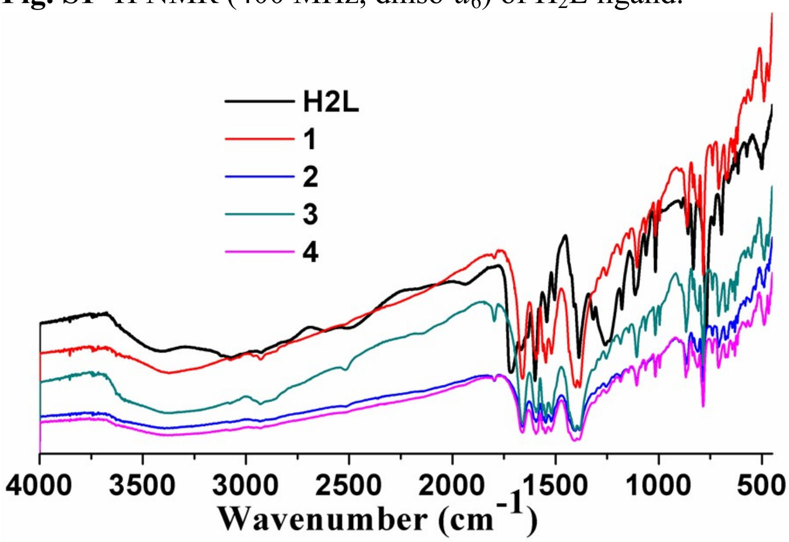

Fig. S2 IR absorption of H_2L ligand and Ln-MOFs **1**–**4**.

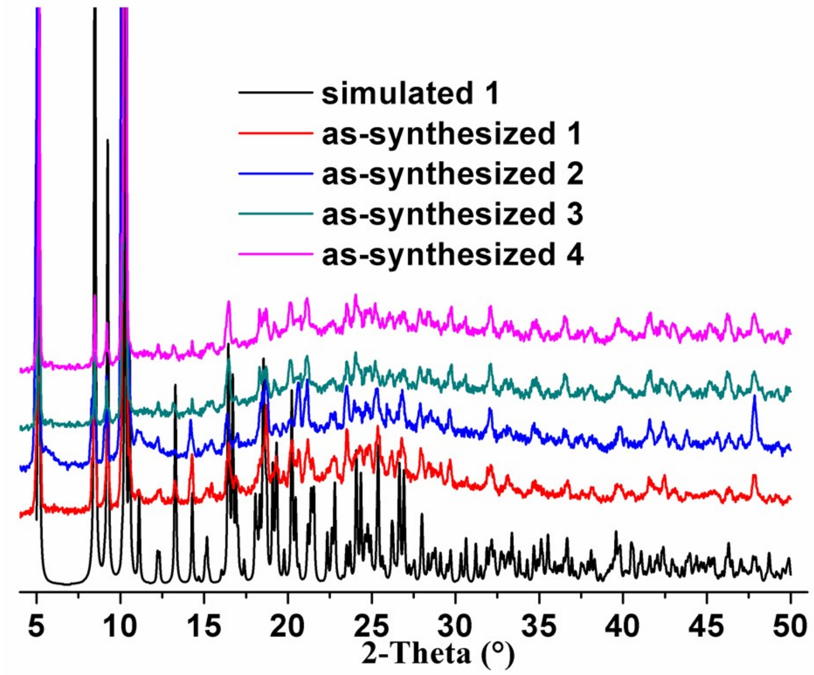

Fig. S3 Powder XRD profiles of simulated **1** and as-synthesized Ln-MOFs **1**–**4**.

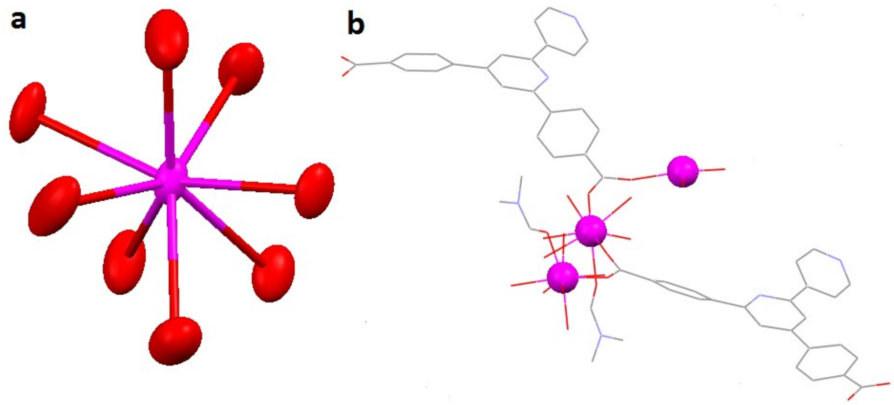

Fig. S4 (a) The distorted dodecahedral coordination geometry of Eu^{3+} centre, (b) the trinuclear secondary building unit in **1**.

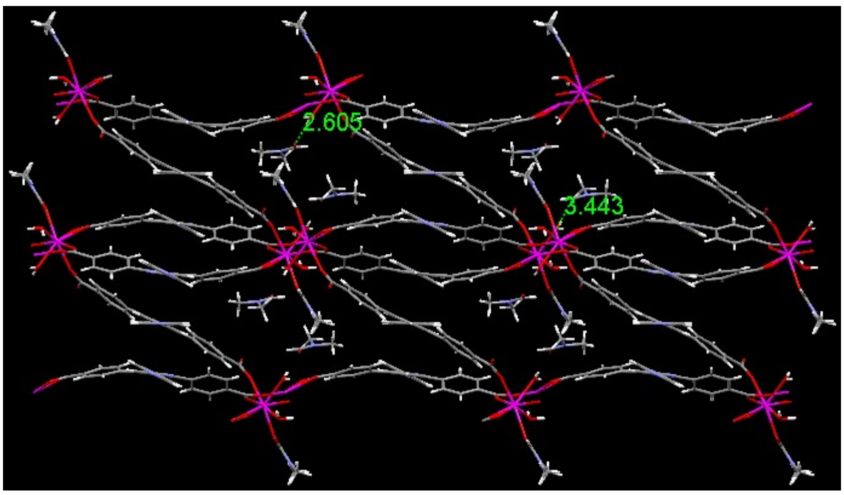

Fig. S5 The supramolecular interactions between guest DMF molecules and the coordinating H_2O molecules in **1**.

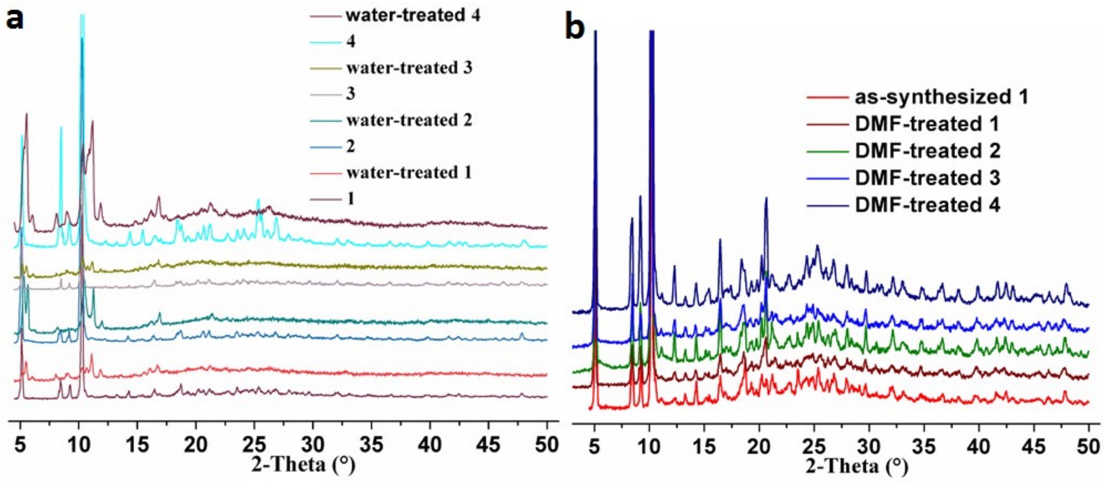

Fig. S6 Powder XRD profiles of (a) as-synthesized Ln-MOFs **1**–**4** and water-treated **1**–**4**, (b) as-synthesized **1** and DMF-treated **1**–**4**.

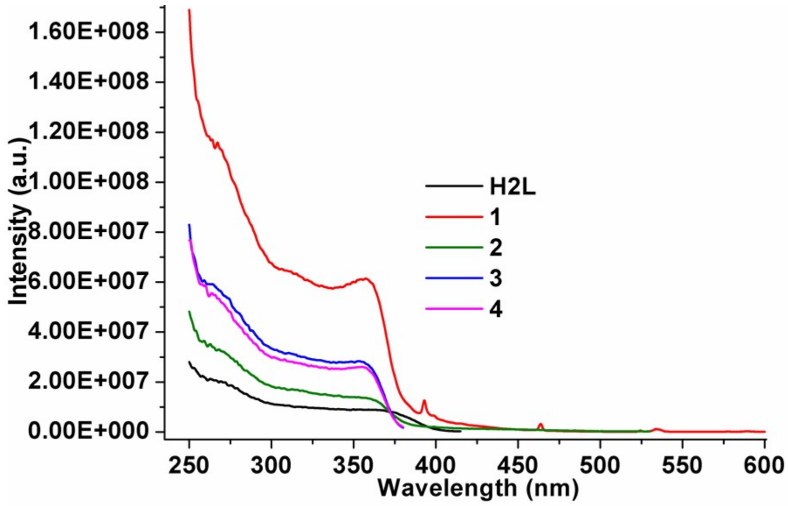

Fig. S7 Solid-state excitation spectra of H_2L ligand and Ln-MOFs **1**–**4**.

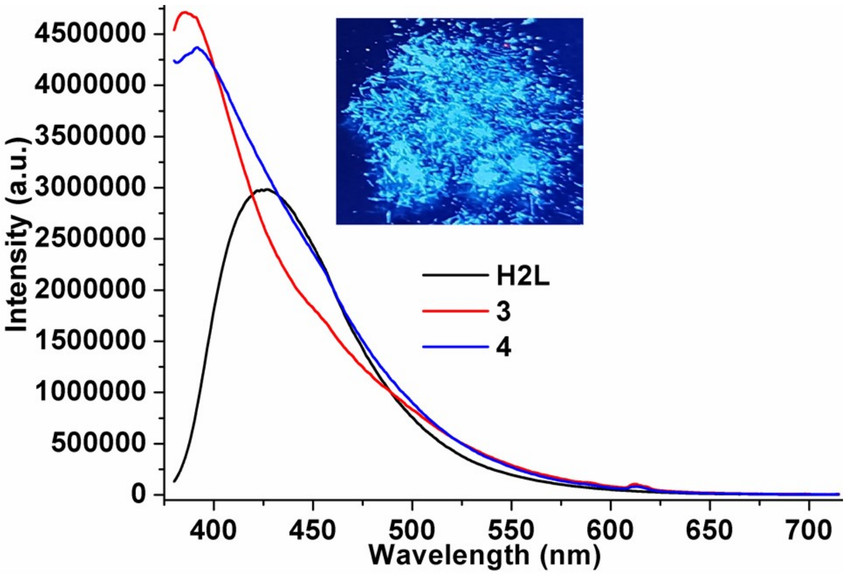

Fig. S8 Solid-state emission spectra of H_2L ligand, and Ln-MOFs **3** and **4** (the inset is the corresponding photograph of **4** taken under 254 nm UV irradiation).

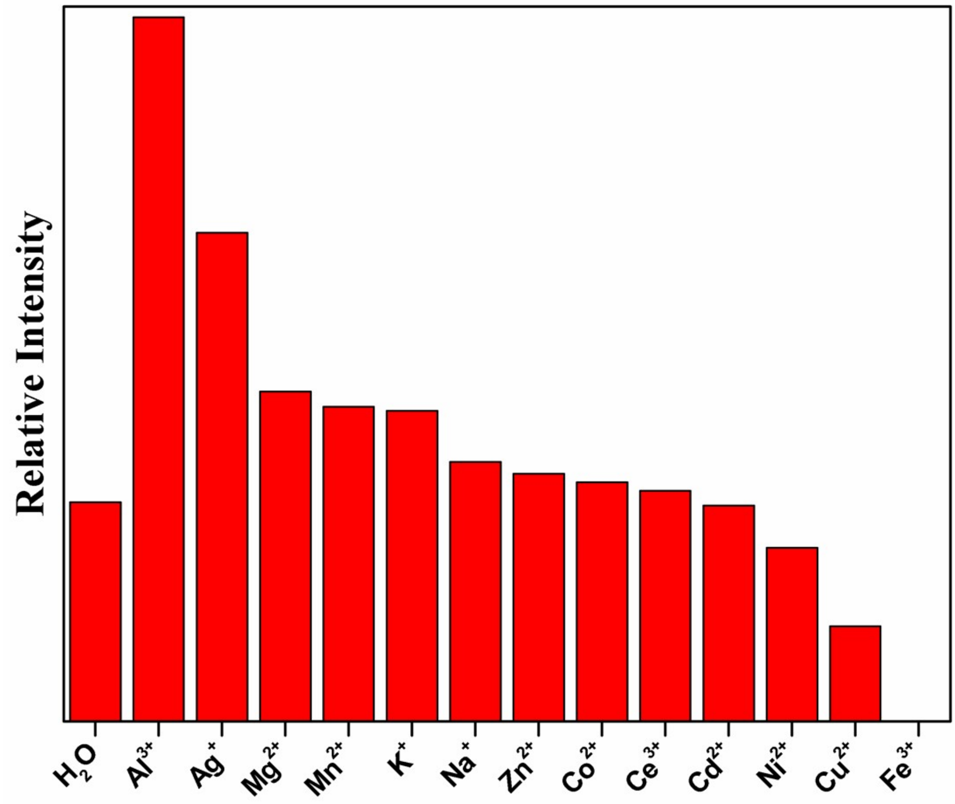

Fig. S9 The bar chart of luminescent intensities at maximum emission wavelength (*ca.* 613 nm) of **1** suspended in different metal ion aqueous solutions.

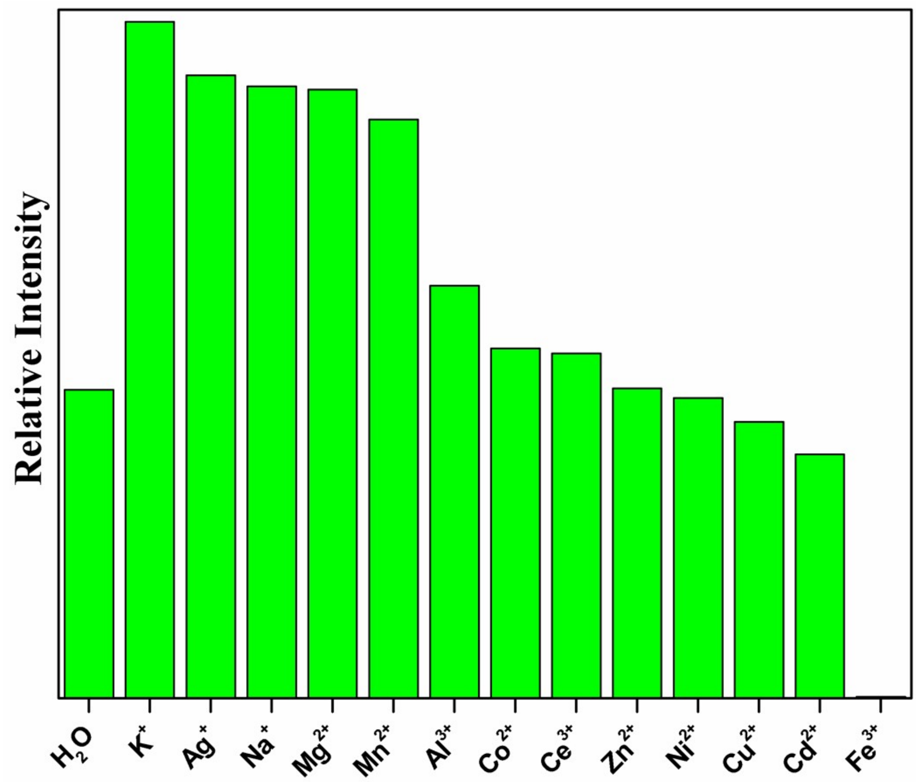

Fig. S10 The bar chart of luminescent intensities at maximum emission wavelength (*ca.* 542 nm) of **2** suspended in different metal ion aqueous solutions.

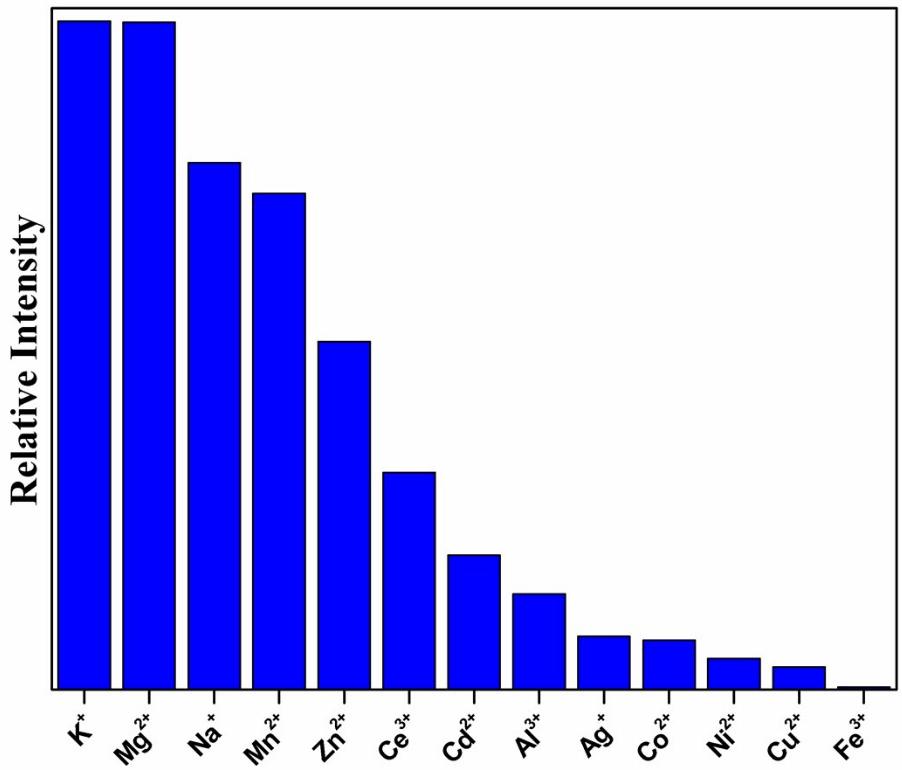

Fig. S11 The bar chart of luminescent intensities at maximum emission wavelength (*ca.* 386 nm) of **3** suspended in different metal ion aqueous solutions.

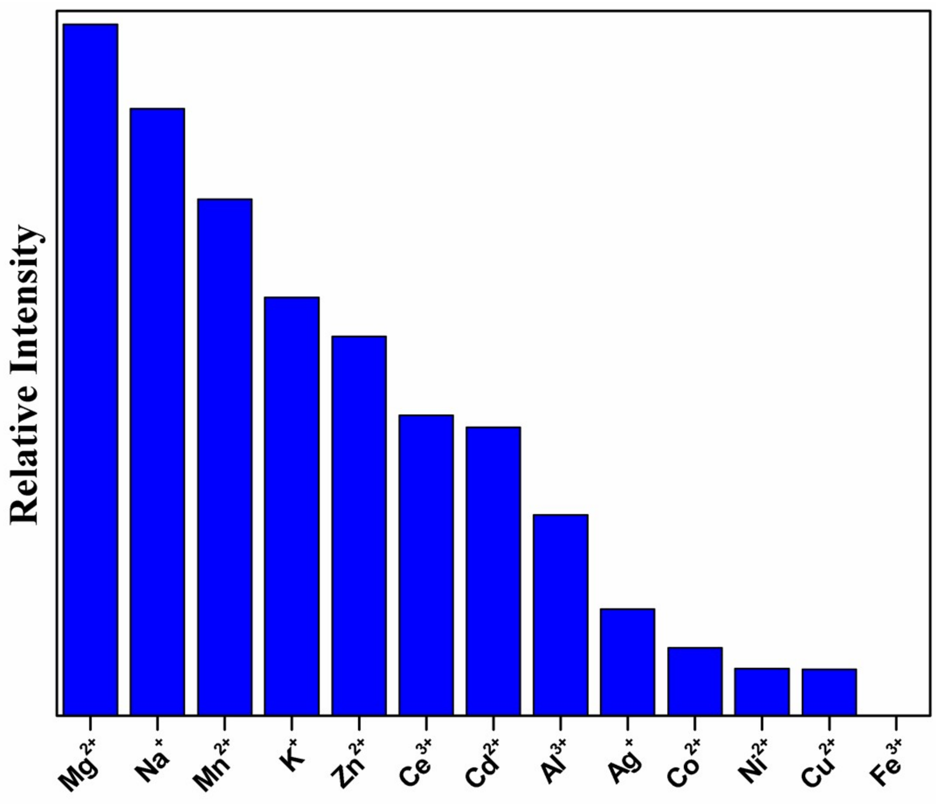

Fig. S12 The bar chart of luminescent intensities at maximum emission wavelength (*ca.* 392 nm) of **4** suspended in different metal ion aqueous solutions.

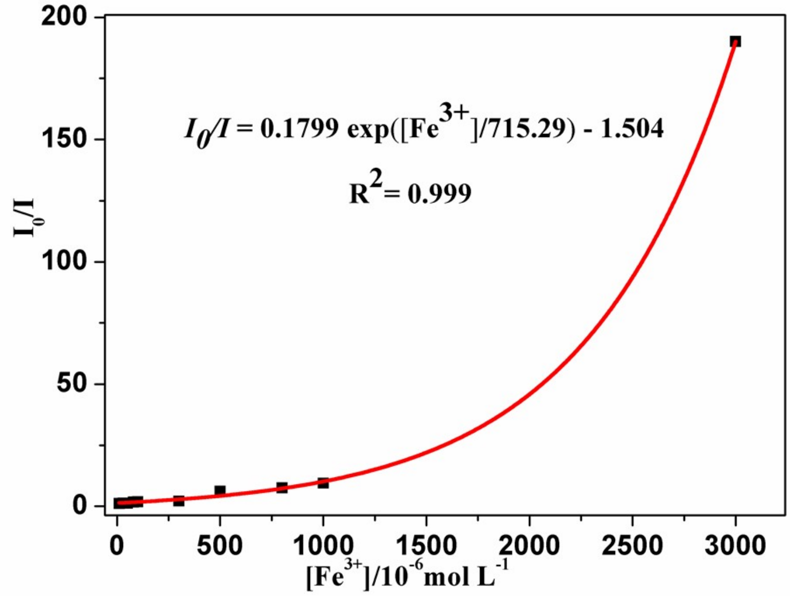

Fig. S13 Plot of I_0/I versus concentration of Fe^{3+} ion aqueous solutions for **1**.

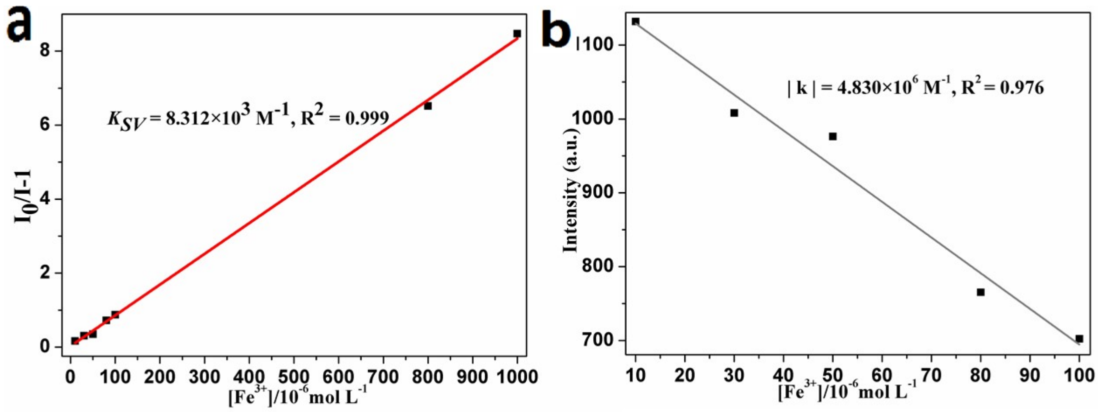

Fig. S14 (a) Stern–Volmer plot of $I_0/I-1$ versus concentration of Fe^{3+} ion aqueous solutions for **1**. (b) Luminescent intensity versus concentration of Fe^{3+} ion aqueous solutions for **1**.

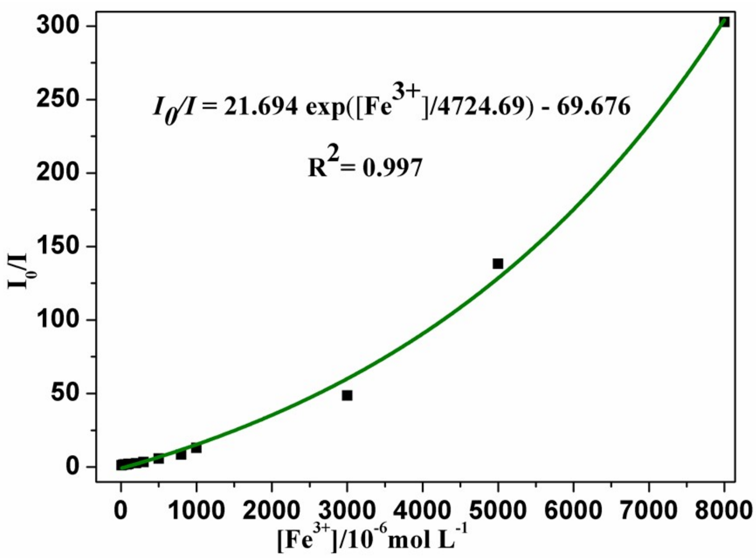

Fig. S15 Plot of I_0/I versus concentration of Fe^{3+} ion aqueous solutions for **2**.

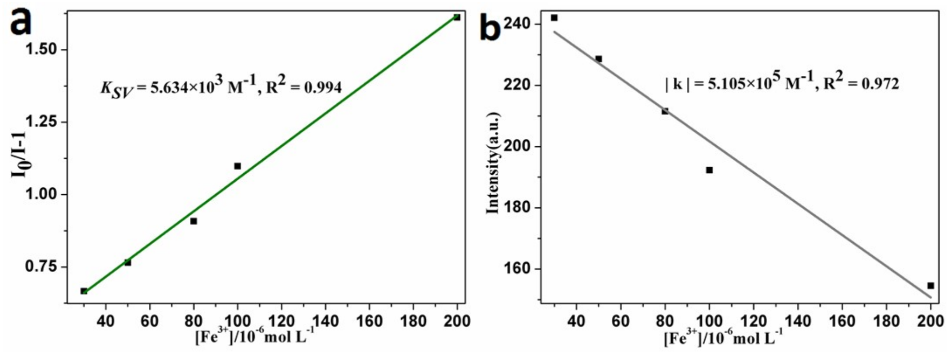

Fig. S16 (a) Stern–Volmer plot of $I_0/I{-}1$ versus concentration of Fe^{3+} ion aqueous solutions for **2**. (b) Luminescent intensity versus concentration of Fe^{3+} ion aqueous solutions for **2**.

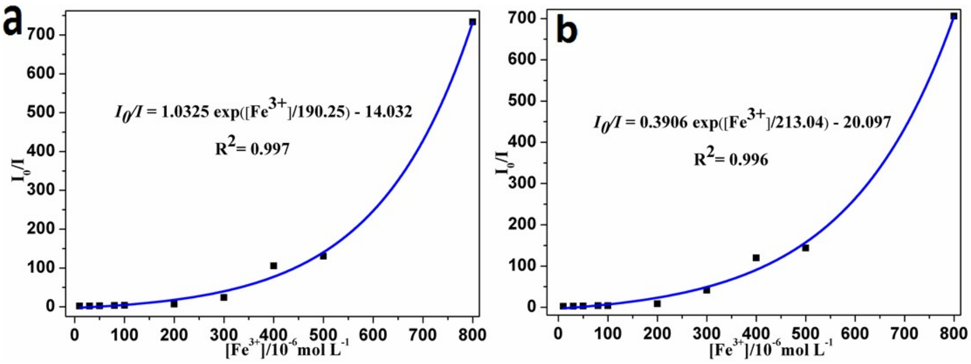

Fig. S17 Plot of I_0/I versus concentration of Fe^{3+} ion aqueous solutions for **3** (a) and **4** (b).

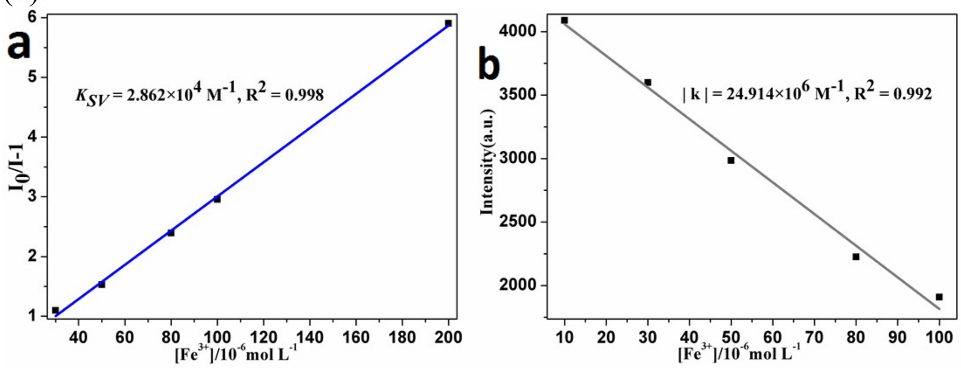

Fig. S18 (a) Stern–Volmer plot of $I_0/I{-}1$ versus concentration of Fe^{3+} ion aqueous solutions for **3**. (b) Luminescent intensity versus concentration of Fe^{3+} ion aqueous solutions for **3**.

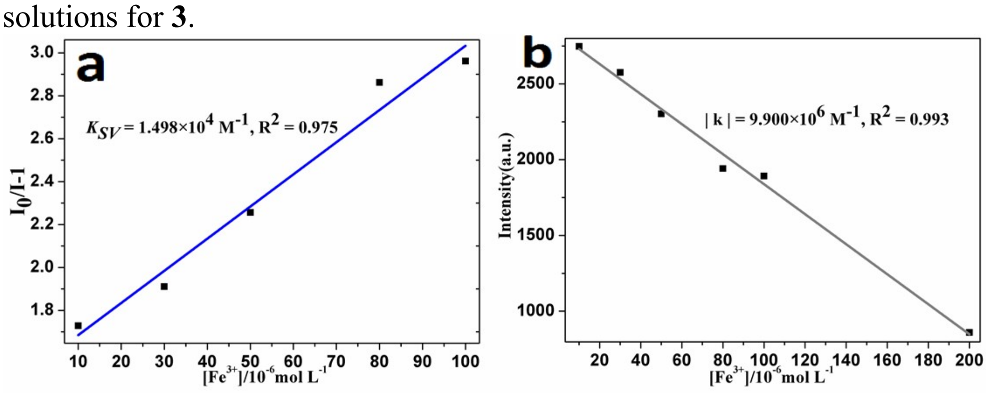

Fig. S19 (a) Stern–Volmer plot of $I_0/I{-}1$ versus concentration of Fe^{3+} ion aqueous solutions for **4**. (b) Luminescent intensity versus concentration of Fe^{3+} ion aqueous solutions for **4**.

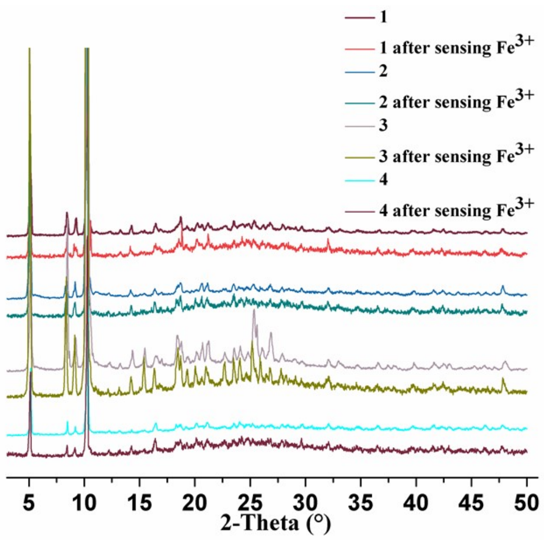

Fig. S20 PXRD patterns of Ln-MOFs **1–4** treated by $Fe(NO_3)_3$ aqueous solutions, indicating that **1–4** retain their frameworks after immersed in $Fe(NO_3)_3$ aqueous solutions.

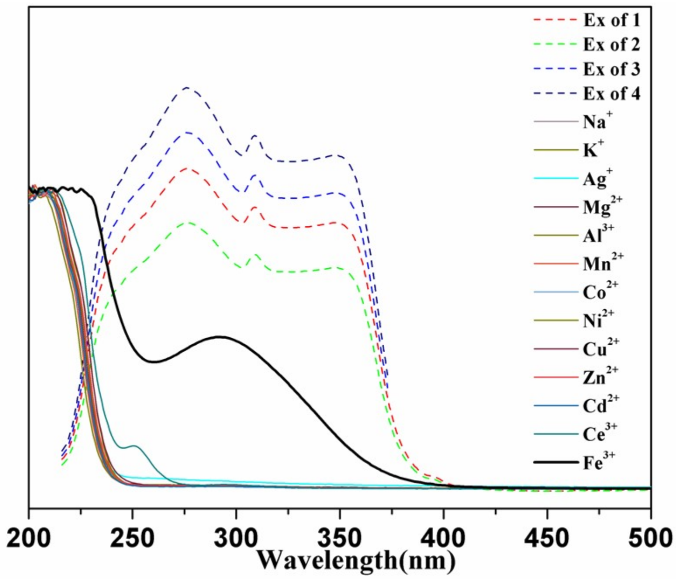

Fig. S21 UV-vis adsorption spectra of different $M(NO_3)_X$ aqueous solutions, and the excitation spectra of Ln-MOFs **1–4**.

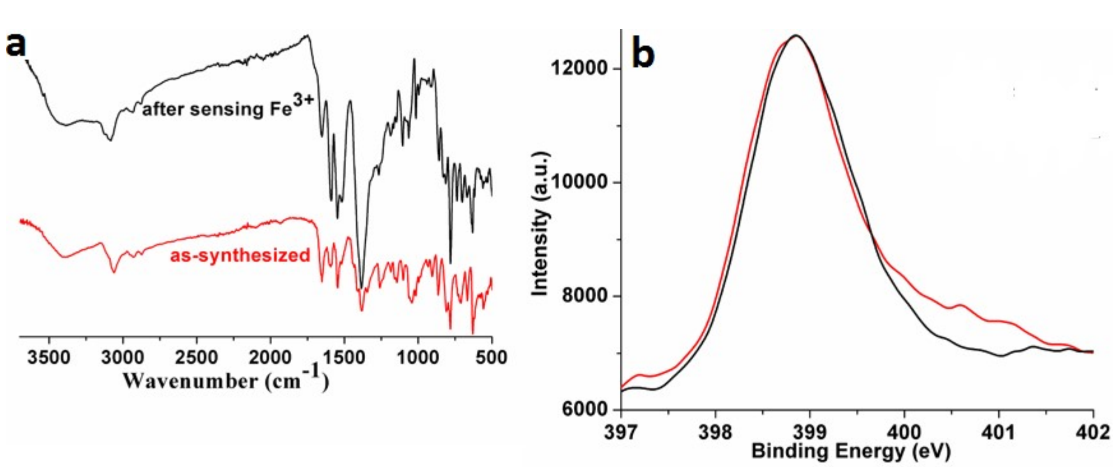

Fig. S22 (a) IR absorption and (b) N1s spectrum of **1** before (red line) and after (black line) sensing Fe^{3+} ion.

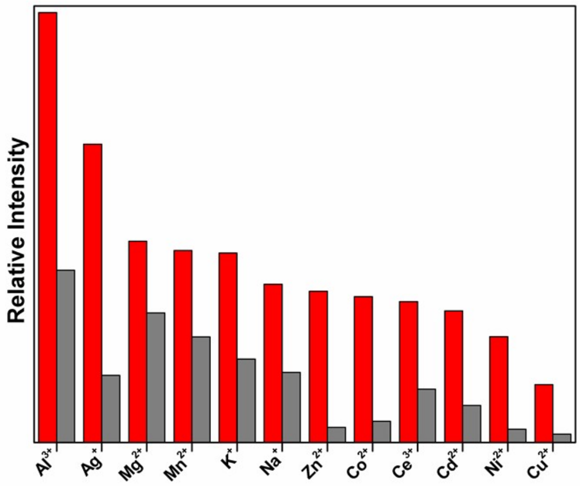

Fig. S23 Luminescence intensities of **1** (λ_{ex} = 365 nm) in different metal ions (1×10^{-2} mol L^{-1}, red bar chart) and corresponding mixed-metal solutions containing Fe^{3+} ions (1× 10^{-3} mol L^{-1}, gray bar chart). Note: Because **1** could possess inferior selectivity for sensing Fe^{3+} ions, it shows weak quenching effect compared those without other interference ions.

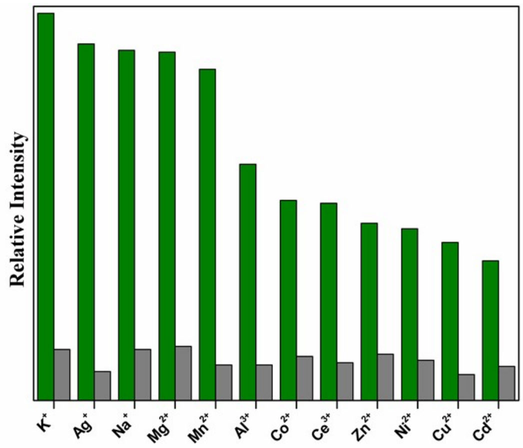

Fig. S24 Luminescence intensities of **2** (λ_{ex} = 365 nm) in different metal ions (1×10^{-2} mol L^{-1}, green bar chart) and corresponding mixed-metal solutions containing Fe^{3+} ions (1× 10^{-3} mol L^{-1}, gray bar chart).

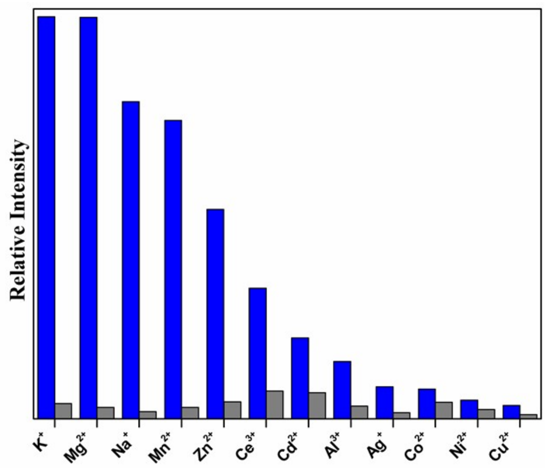

Fig. S25 Luminescence intensities of **3** (λ_{ex} = 300 nm) in different metal ions (1×10^{-2} mol L^{-1}, blue bar chart) and corresponding mixed-metal solutions containing Fe^{3+} ions (1× 10^{-3} mol L^{-1}, gray bar chart).

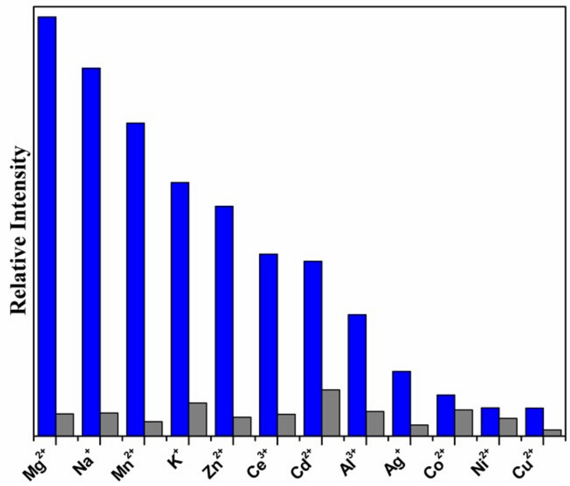

Fig. S26 Luminescence intensities of **4** (λ_{ex} = 300 nm) in different metal ions (1×10^{-2} mol L^{-1}, blue bar chart) and corresponding mixed-metal solutions containing Fe^{3+} ions (1×10^{-3} mol L^{-1}, gray bar chart).

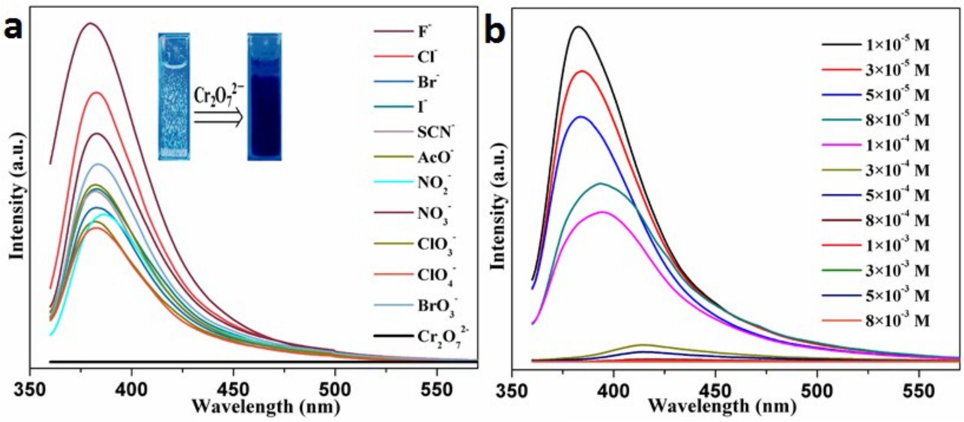

Fig. S27 Luminescence spectra (λ_{ex}= 345 nm) of **3** dispersed in (a) different anionic aqueous solutions (The inset photographs taken under 254 nm UV irradiation, showing the quenching effects before (left) and after (right) dispersion in the $Cr_2O_7^{2-}$ aqueous solution.), and (b) various concentrations of the $Cr_2O_7^{2-}$ aqueous solutions.

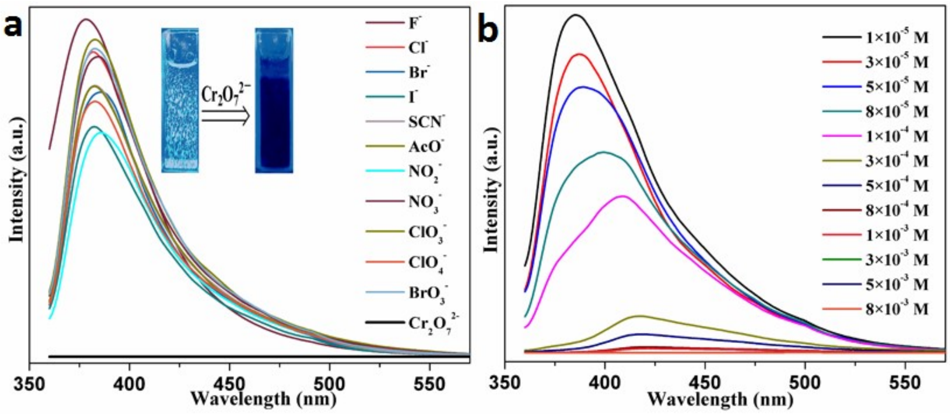

Fig. S28 Luminescence spectra (λ_{ex}= 345 nm) of **4** dispersed in (a) different anionic aqueous solutions (The inset photographs taken under 254 nm UV irradiation, showing the quenching effects before (left) and after (right) dispersion in the $Cr_2O_7^{2-}$ aqueous solution.), and (b) various concentrations of the $Cr_2O_7^{2-}$ aqueous solutions.

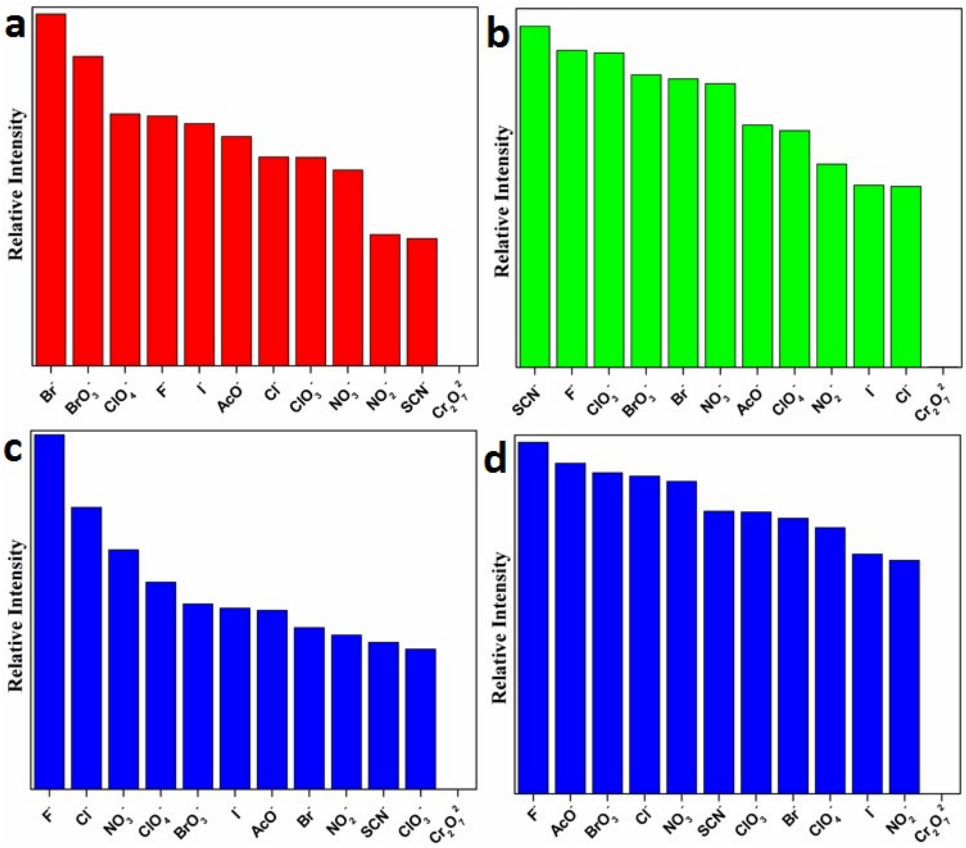

Fig. S29 The bar chart of luminescent intensities of samples suspended in different anionic aqueous solutions with maximum emission wavelength at 613 nm of **1** (a), 542 nm of **2** (b), 386 nm of **3** (c) and 392 nm of **4** (d).

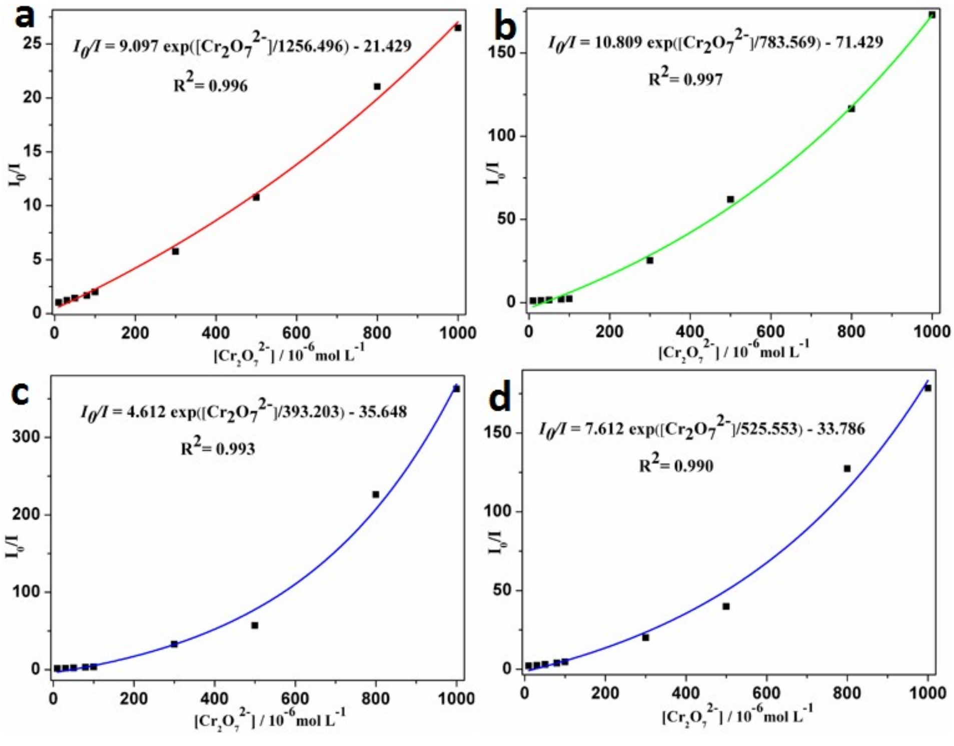

Fig. S30 Plot of I_0/I versus concentration of $Cr_2O_7^{2-}$ anion aqueous solutions for **1** (a), **2** (b), **3** (c) and **4** (d).

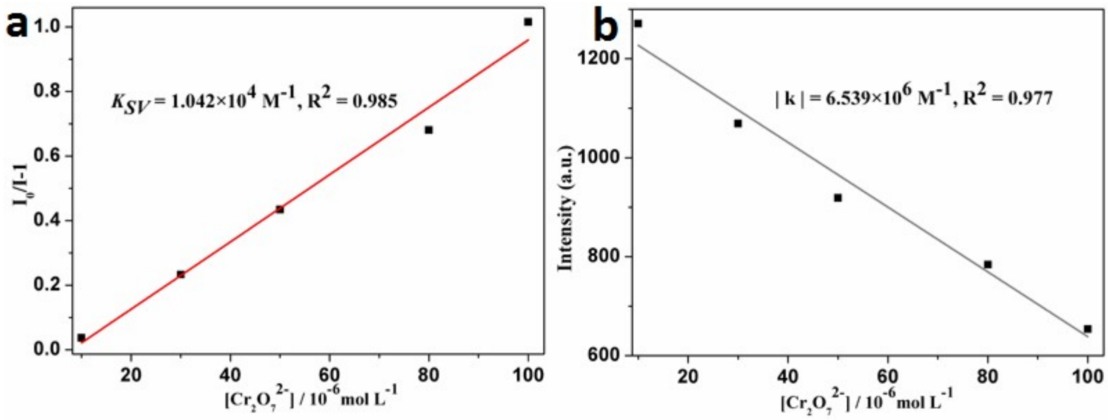

Fig. S31 (a) Stern–Volmer plot of $I_0/I-1$ versus concentration of $Cr_2O_7^{2-}$ anion aqueous solutions for **1**. (b) Luminescent intensity versus concentration of $Cr_2O_7^{2-}$ anion aqueous solutions for **1**.

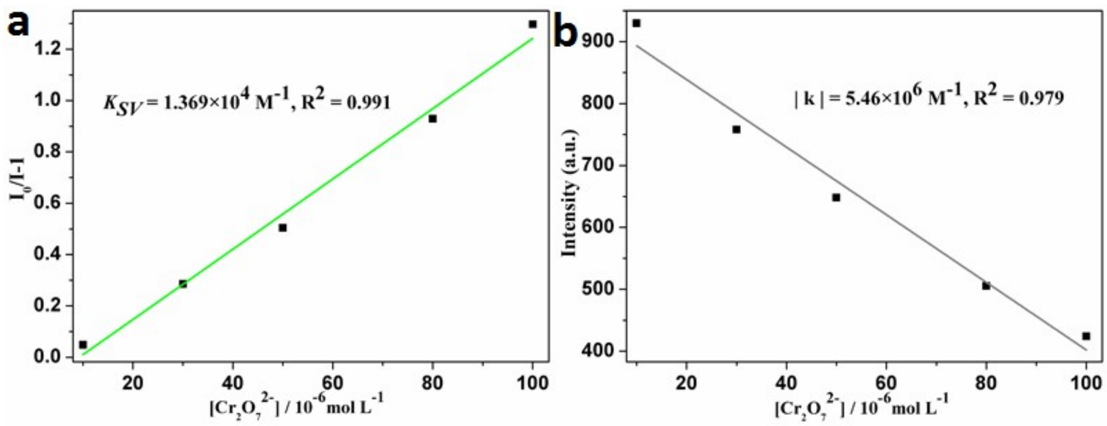

Fig. S32 (a) Stern–Volmer plot of $I_0/I-1$ versus concentration of $Cr_2O_7^{2-}$ anion aqueous solutions for **2**. (b) Luminescent intensity versus concentration of $Cr_2O_7^{2-}$ anion aqueous solutions for **2**.

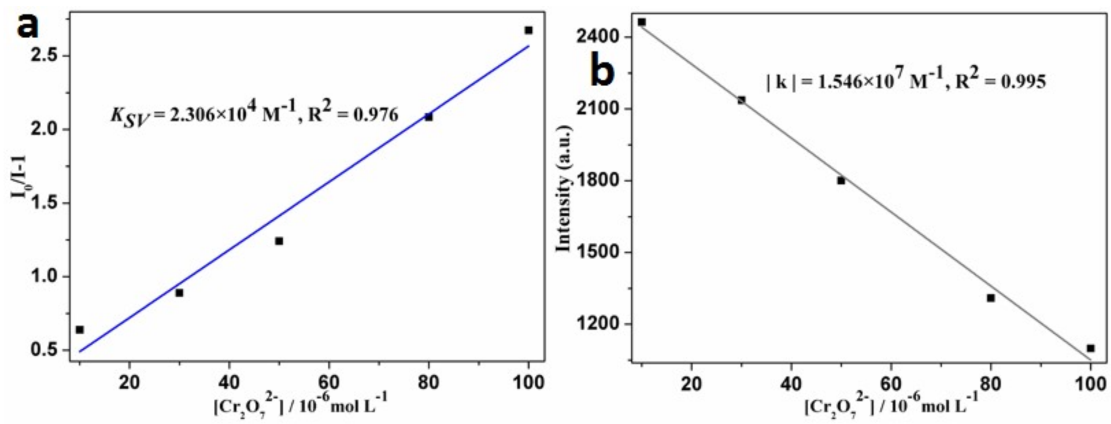

Fig. S33 (a) Stern–Volmer plot of $I_0/I-1$ versus concentration of $Cr_2O_7^{2-}$ anion aqueous solutions for **3**. (b) Luminescent intensity versus concentration of $Cr_2O_7^{2-}$ anion aqueous solutions for **3**.

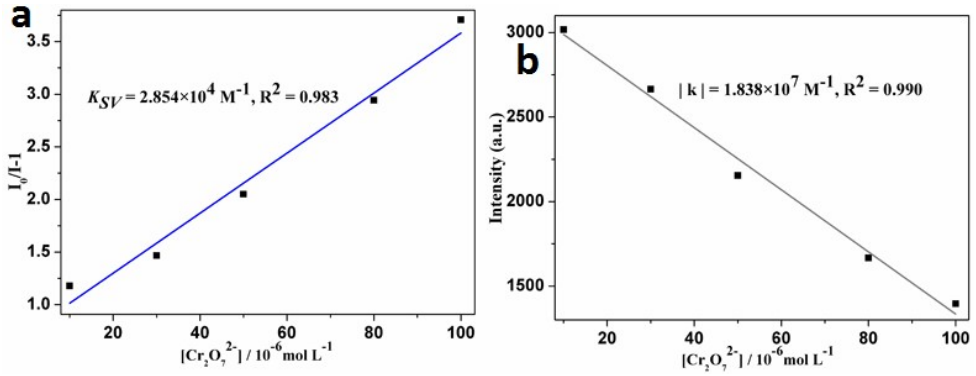

Fig. S34 (a) Stern–Volmer plot of $I_0/I{-}1$ versus concentration of $Cr_2O_7^{2-}$ anion aqueous solutions for **4**. (b) Luminescent intensity versus concentration of $Cr_2O_7^{2-}$ anion aqueous solutions for **4**.

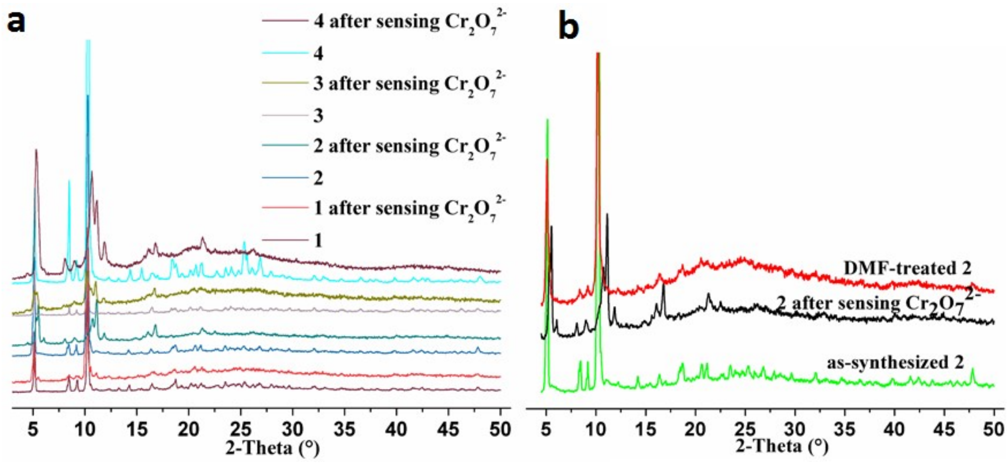

Fig. S35 PXRD patterns of (a) Ln-MOFs **1**–**4** treated by $K_2Cr_2O_7$ aqueous solutions, and (b) re-solvated **2** by DMF/H_2O solution.

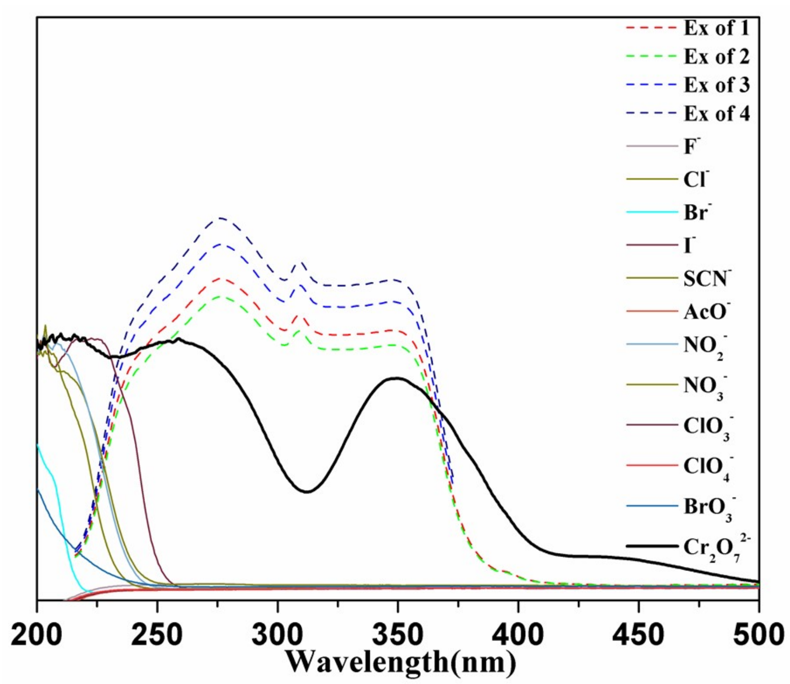

Fig. S36 UV-vis adsorption spectra of different K_yA aqueous solutions, and the excitation spectra of Ln-MOFs **1**–**4**.

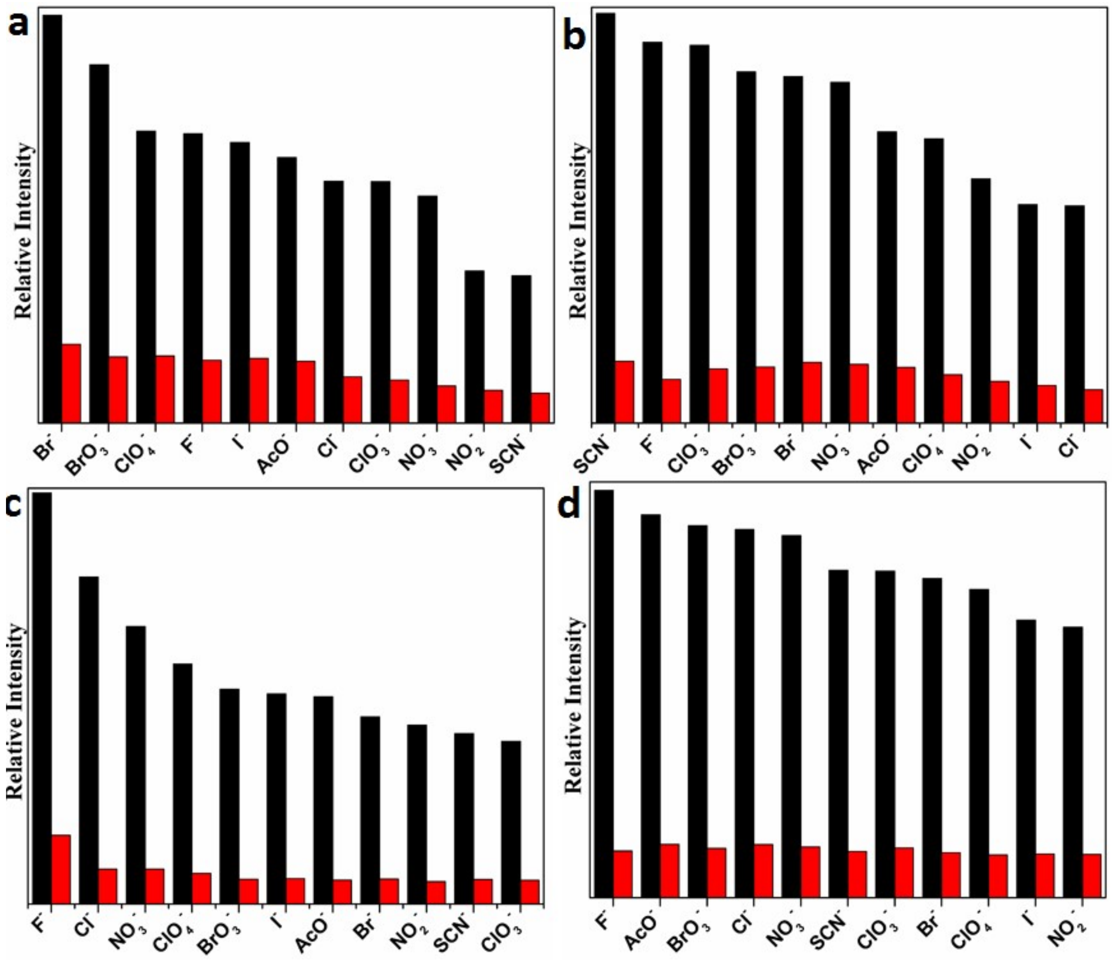

Fig. S37 Luminescence intensities of **1** (a), **2** (b), **3** (c) and **4** (d) in different anion aqueous solutions (1×10^{-2} mol L^{-1}, black bar chart) and their corresponding mixed-anion solutions containing $Cr_2O_7^{2-}$ anions (1×10^{-3} mol L^{-1}, red bar chart).